García-Ruiz, A., Dominguez-Lopez, A., Pastor-Graells, J.,Martins, H.F., Martin-Lopez, S. and González-Herraez, M.,2018, " Long-range distributed optical fiber hot-wire anemometer based on chirped-pulse ΦOTDR", Optics Express, v.26, issue 1, pp. 463-476.

Available at: https://doi.org/10.1364/OE.26.000463

Long-range distributed optical fiber hot-wire anemometer based on chirped-pulse ΦOTDR

Andres Garcia-Ruiz,[1,*] Alejandro Dominguez-Lopez,[1] Juan Pastor-Graells,[1] Hugo F. Martins,[2] Sonia Martin-Lopez,[1] and Miguel Gonzalez-Herraez[1]

[1] *Dpto. de Electrónica, University of Alcalá, 28805, Alcalá de Henares (Madrid), Spain*
[2] *FOCUS S. L., C/ Orellana, 1, 1º Izq., 28004, Madrid, Spain*
[*] *andres.garciaruiz@uah.es*

Abstract: We demonstrate a technique allowing to develop a fully distributed optical fiber hot-wire anemometer capable of reaching a wind speed uncertainty of ≈ ±0.15 m/s (±0.54 km/h) at only 60 mW/m of dissipated power in the sensing fiber, and within only four minutes of measurement time. This corresponds to similar uncertainty values than previous papers on distributed optical fiber anemometry but requires two orders of magnitude smaller dissipated power and covers at least one order of magnitude longer distance. This breakthrough is possible thanks to the extreme temperature sensitivity and single-shot performance of chirped-pulse phase-sensitive optical time domain reflectometry (ΦOTDR), together with the availability of metal-coated fibers. To achieve these results, a modulated current is fed through the metal coating of the fiber, causing a modulated temperature variation of the fiber core due to Joule effect. The amplitude of this temperature modulation is strongly dependent on the wind speed at which the fiber is subject. Continuous monitoring of the temperature modulation along the fiber allows to determine the wind speed with singular low power injection requirements. Moreover, this procedure makes the system immune to temperature drifts of the fiber, potentially allowing for a simple field deployment. Being a much less power-hungry scheme, this method also allows for monitoring over much longer distances, in the orders of 10s of km. We expect that this system can have application in dynamic line rating and lateral wind monitoring in railway catenary wires.

OCIS codes: (060.2370) Fiber optics sensors; (290.5870) Scattering, Rayleigh; (280.0280) Remote sensing and sensors; (120.4825) Optical time domain reflectometry; (280.7250) Velocimetry; (999.9999) Anemometry.

References and links

1. L. V. King, "On the convection of heat from small cylinders in a stream of fluid: determination of the convection constants of small platinum wires with applications to hot-wire anemometry," Philosophical Transactions of the Royal Society A **214**, 373–432 (1914).
2. H. H. Bruun, *Hot-wire Anemometry-principles and Signal Analysis* (Oxford Science Publications, 1995).
3. J. Mandle, "System for determining the airspeed of an aircraft," US Patent 8,718,971 (2014).
4. R. Gawthorpe, "Wind effects on ground transportation," Journal of Wind Engineering and Industrial Aerodynamics **52**, 73–92 (1994).
5. C. Proppe and C. Wetzel, "Overturning probability of railway vehicles under wind gust loads," in *IUTAM Symposium on Dynamics and Control of Nonlinear Systems with Uncertainty,* vol. 2 (Springer, 2007), pp. 23–32.
6. O. Chabart and J.-L. Lilien, "Galloping of electrical lines in wind tunnel facilities," Journal of Wind Engineering and Industrial Aerodynamics **74**, 967–976 (1998).
7. J. Wang and J.-L. Lilien, "Overhead electrical transmission line galloping. A full multi-span 3-DOF model, some applications and design recommendations," IEEE Transactions on Power Delivery **13**, 909–916 (1998).
8. G.-M. Ma, C.-R. Li, J. Jiang, J.-Y. Liang, Y.-T. Luo, and Y.-C. Cheng, "A passive optical fiber anemometer for wind speed measurement on high-voltage overhead transmission lines," IEEE Transactions on Instrumentation and Measurement **61**, 539–544 (2012).
9. S. D. Foss and R. A. Maraio, "Dynamic line rating in the operating environment," IEEE Transactions on Power Delivery **5**, 1095–1105 (1990).
10. Y. Yang, D. Divan, R. G. Harley, and T. G. Habetler, "Power line sensornet - A new concept for power grid monitoring," in *Power Engineering Society General Meeting,* (IEEE, 2006).
11. A. Michiorri, H.-M. Nguyen, S. Alessandrini, J. B. Bremnes, S. Dierer, E. Ferrero, B.-E. Nygaard, P. Pinson, N. Thomaidis, and S. Uski, "Forecasting for dynamic line rating," Renewable & Sustainable Energy Reviews **52**,

1713–1730 (2015).
12. J. Fu, S. Abbott, B. Fox, D. J. Morrow, and S. Abdelkader, "Wind cooling effect on dynamic overhead line ratings," in *Universities Power Engineering Conference*, (IEEE, 2010), pp. 1–6.
13. B. Culshaw and A. Kersey, "Fiber-optic sensing: a historical perspective," Journal of Lightwave Technology **26**, 1064–1078 (2008).
14. L. Palmieri and L. Schenato, "Distributed optical fiber sensing based on Rayleigh scattering," The Open Optics Journal **7** (2013).
15. L. Schenato, A. Pasuto, A. Galtarossa, and L. Palmieri, "Optical fiber load sensor based on a semi-auxetic structure: a proof of concept," in *Sixth European Workshop on Optical Fibre Sensors*, (International Society for Optics and Photonics, 2016), pp. 99160N–99160N.
16. L. X. Chen, X. G. Huang, J. H. Zhu, G. C. Li, and S. Lan, "Fiber magnetic-field sensor based on nanoparticle magnetic fluid and Fresnel reflection," Optics letters **36**, 2761–2763 (2011).
17. L. Xia, L. Li, W. Li, T. Kou, and D. Liu, "Novel optical fiber humidity sensor based on a no-core fiber structure," Sensors and Actuators A: Physical **190**, 1–5 (2013).
18. M. Calcerrada, C. García-Ruiz, and M. González-Herráez, "Chemical and biochemical sensing applications of microstructured optical fiber-based systems," Laser & Photonics Reviews **9**, 604–627 (2015).
19. Y. Antman, A. Clain, Y. London, and A. Zadok, "Optomechanical sensing of liquids outside standard fibers using forward stimulated Brillouin scattering," Optica **3**, 510–516 (2016).
20. A. Garcia-Ruiz, J. Pastor-Graells, H. F. Martins, K. H. Tow, L. Thévenaz, S. Martin-Lopez, and M. Gonzalez-Herraez, "Distributed photothermal spectroscopy in microstructured optical fibers: towards high-resolution mapping of gas presence over long distances," Opt. Express **25**, 1789–1805 (2017).
21. J. Pastor-Graells, H. F. Martins, A. Garcia-Ruiz, S. Martín-López, and M. Gonzalez-Herraez, "Single-shot distributed temperature and strain tracking using direct detection phase-sensitive OTDR with chirped pulses," Opt. Express **24**, 13121–13133 (2016).
22. A. Garcia-Ruiz, H. Martins, J. Pastor-Graells, S. Martin-Lopez, and M. Gonzalez-Herraez, "Single-Shot True Distributed Strain Variation Measurements Over >10 km Using Phase-Sensitive OTDR with Chirped Pulses," in *Asia-Pacific Optical Sensors Conference*, (Optical Society of America, 2016), pp. Th3A–2.
23. T. L. Bergman, F. P. Incropera, D. P. DeWitt, and A. S. Lavine, *Fundamentals of Heat and Mass Transfer* (John Wiley & Sons, 2011).
24. V. T. Morgan, "The overall convective heat transfer from smooth circular cylinders," Advances in Heat Transfer **11**, 199–264 (1975).
25. A. Abdel-Rahman, "On the yaw-angle characteristics of hot-wire anemometers," Flow Measurement and Instrumentation **6**, 271–278 (1995).
26. L. Di Mare, T. Jelly, and I. Day, "Angular response of hot wire probes," Measurement Science and Technology **28**, 035303 (2017).
27. T. Chen, Q. Wang, B. Zhang, R. Chen, and K. P. Chen, "Distributed flow sensing using optical hot-wire grid," Opt. Express **20**, 8240–8249 (2012).
28. G. Pitt, A. Prabakaran, R. Williamson, D. Wilson, and D. Batchelder, "Optical fibre flowmeters," in 2^{nd} *International Conference on Optical Fiber Sensors*, (International Society for Optics and Photonics, 1984), pp. 23–28.
29. G. Liu, W. Hou, W. Qiao, and M. Han, "Fast-response fiber-optic anemometer with temperature self-compensation," Opt. Express **23**, 13562–13570 (2015).
30. S. Gao, A. P. Zhang, H.-Y. Tam, L. Cho, and C. Lu, "All-optical fiber anemometer based on laser heated fiber Bragg gratings," Opt. Express **19**, 10124–10130 (2011).
31. Y. Liu, W. Peng, X. Zhang, Y. Liang, Z. Gong, and M. Han, "Fiber-optic anemometer based on distributed Bragg reflector fiber laser technology," IEEE Photonics Technology Letters **25**, 1246–1249 (2013).
32. X. Wang, X. Dong, Y. Zhou, K. Ni, J. Cheng, and Z. Chen, "Hot-wire anemometer based on silver-coated fiber Bragg grating assisted by no-core fiber," IEEE Photonics Technology Letters **25**, 2458–2461 (2013).
33. L. C. Bobb, J. P. Davis, A. Samouris, and D. C. Larson, "An optical fiber hot-wire anemometer," in "OE/FIBERS'89," (International Society for Optics and Photonics, 1990), pp. 567–572.
34. M. T. Wylie, A. W. Brown, and B. G. Colpitts, "Distributed hot-wire anemometry based on Brillouin optical time-domain analysis," Opt. Express **20**, 15669–15678 (2012).
35. L. Zhou, F. Wang, X. Wang, Y. Pan, Z. Sun, J. Hua, and X. Zhang, "Distributed strain and vibration sensing system based on phase-sensitive OTDR," IEEE Photonics Technology Letters **27**, 1884–1887 (2015).
36. Y. Koyamada, M. Imahama, K. Kubota, and K. Hogari, "Fiber-optic distributed strain and temperature sensing with very high measurand resolution over long range using coherent OTDR," Journal of Lightwave Technology **27**, 1142–1146 (2009).
37. G. Tu, X. Zhang, Y. Zhang, F. Zhu, L. Xia, and B. Nakarmi, "The Development of an ΦOTDR System for Quantitative Vibration Measurement," IEEE Photonics Technology Letters **27**, 1349–1352 (2015).
38. A. Garcia-Ruiz, J. Pastor-Graells, H. F. Martins, S. Martin-Lopez, and M. Gonzalez-Herraez, "Speckle Analysis Method for Distributed Detection of Temperature Gradients With ΦOTDR," IEEE Photonics Technology Letters **28**, 2000–2003 (2016).
39. S. Liehr, Y. S. Muanenda, S. Münzenberger, and K. Krebber, "Relative change measurement of physical quantities using dual-wavelength coherent OTDR," Opt. Express **25**, 720–729 (2017).

40. G. Failleau, O. Beaumont, R. Razouk, S. Delepine-Lesoille, M. Landolt, B. Courthial, J. Hénault, F. Martinot, J. Bertrand, and B. Hay, "A metrological comparison of Raman-distributed temperature sensors," Measurement **116**, 18–24 (2018).
41. M. Wang, H. Wu, M. Tang, Z. Zhao, Y. Dang, C. Zhao, R. Liao, W. Chen, S. Fu, C. Yang *et al.*, "Few-mode fiber based Raman distributed temperature sensing," Optics Express **25**, 4907–4916 (2017).
42. X. Angulo-Vinuesa, A. Dominguez-Lopez, A. Lopez-Gil, J. D. Ania-Castañón, S. Martin-Lopez, and M. Gonzalez-Herraez, "Limits of BOTDA range extension techniques," (IEEE Sensors, 2015).
43. Y. Dang, Z. Zhao, M. Tang, C. Zhao, L. Gan, S. Fu, T. Liu, W. Tong, P. P. Shum, and D. Liu, "Towards large dynamic range and ultrahigh measurement resolution in distributed fiber sensing based on multicore fiber," Opt. Express **25**, 20183–20193 (2017).
44. J. Pastor-Graells, J. Nuño, M. R. Fernández-Ruiz, A. Garcia-Ruiz, H. F. Martins, S. Martin-Lopez, and M. Gonzalez-Herraez, "Chirped-pulse Phase-sensitive Reflectometer Assisted by First Order Raman Amplification," Journal of Lightwave Technology **35**, 4677–4683 (2017).
45. H. Zhu, C. Pan, and X. Sun, "Vibration pattern recognition and classification in OTDR based distributed optical-fiber vibration sensing system," in "SPIE Smart Structures and Materials+ Nondestructive Evaluation and Health Monitoring," (International Society for Optics and Photonics, 2014), pp. 906205–906205.
46. Q. Sun, H. Feng, X. Yan, and Z. Zeng, "Recognition of a phase-sensitivity OTDR sensing system based on morphologic feature extraction," Sensors **15**, 15179–15197 (2015).

1. Introduction

For many years, the technique known as *hot-wire anemometry* (HWA) has been one of the most widely applied methods for the measurement of flow speeds by exploiting the thermal phenomena involved in fluid dynamics [1, 2]. The traditional HWA technology is based on the dependence of the convective dissipation of heat on the velocity of the fluid that drifts around the hot object. In a typical HWA implementation, a conductive, thin and short wire or film is heated by means of an electrical current and exposed to a fluid in motion. By monitoring the temperature evolution of the hot wire, it is possible to indirectly quantify the flow speed by means of purely thermal or electric measurements.

HWA sensors are nowadays a tool present in many environments, given their convenience for a great amount of applications. The small size of the probe guarantees a low flow modification during the measurement when compared with other sensors. HWA sensors are often employed in large infrastructures for performing continuous wind speed measurements, especially in those sensitive to wind, such as railways, overhead power lines, certain large buildings, bridges, large wind turbines, large aircrafts [3], etc. However, in these structures, addressing only one (or few) measurement points along their whole size turns out to be a strong limitation, since the wind speed profile may vary substantially across the different locations. In such cases, a system capable of monitoring the wind spatial distribution along the distance (i.e. a distributed anemometer) would certainly help in managing the maintenance and risks of failure more efficiently. A particularly interesting example of this is the high-speed railway, where lateral wind may cause disruption in the catenary-pantograph interaction (for moderately high wind loads), and even wagon derailment and overturn in more severe cases [4, 5]. To enhance the safety and reliability of many railway lines, it would be convenient to have the capability of monitoring the magnitude of lateral wind over relatively long sections of e.g. tens of kilometers.

Another interesting potential application of large-scale spatially-resolved anemometry could be the optimization of power transmission along overhead power lines [6–8]. There is an increasing pressure from power grid managers to reduce operating costs by improving the throughput of the power transmission facilities. The line ratings typically applied are well under the maximum possible values, essentially because of reliability and safety concerns. Improved efficiency can be achieved through novel power distribution management paradigm named *dynamic line rating* (DLR) [9, 10]. These models are intended to maximize the electric power delivered through the power cables by tracing the temperature distribution along their length and ensuring that no point goes over the specified temperature rating. The models used in DLR essentially depend on the conductor geometry, the local weather conditions (including wind speed), and the forecast

confidence intervals to which they are subject. It is unquestionable that DLR would greatly take advantage of accurate and real-time weather information along the power line network in order to optimize the ratings for smaller temporal and spatial windows. In particular, precise knowledge of wind speed in every position across the power line would enhance the accuracy of thermal models for line rating, hence allowing for better margins to improve the efficiency of the power transfer [11, 12].

These particular applications would quite surely overload the possibilities of a multi-point hot-wire anemometry system, given the scale of the systems to monitor. It would require installing probe wires (and their corresponding interrogating units, wiring and communications) over a large set of points (covering a distance of tens of km), each sensor requiring 2 or 4 wires, an independent calibration and some kind of communication system. A high sensitivity, truly distributed sensing implementation of the HWA principle could fulfill the requirements of the applications cited above in a more simple and reliable way. The field of HWA still lacks, therefore, of a competitive distributed counterpart. For this reason, a *distributed optical fiber sensor* (DOFS) [13, 14] could represent a good candidate to solve some of the mentioned problems.

Thanks to a wide variety of light propagation phenomena, DOFS can perform measurements at every point along an optical fiber. Through slight modifications of the sensing fiber, sensors for weight [15], electromagnetic field [16], humidity [17], or even chemicals [18–20] have been proposed. On the other hand, the challenge of designing a distributed hot-wire anemometer suits the scope of the fiber-optics sensors community. Pursuing to meet the needs of technologies like DLR, the authors present here a proof of concept for a distributed fiber optical sensor able to provide fast measurements of the speed of a fluid with high sensitivity, immunity to fiber temperature drifts and covering a long distance range. The key point of this paper is the availability of a novel phase-sensitive Optical Time Domain Reflectometry (ΦOTDR) system which employs *chirped* pulses to achieve mK-resolution temperature measurements along kilometer ranges and with update rates of several kHz, formerly developed by the authors [21, 22]. Here we show that having this high-resolution and rapid distributed temperature measurement system allows to achieve the most power-efficient and long-range implementation of a distributed anemometer shown to date.

In the next section we present the physical principles of the traditional HWA technique (2.1) and its fiber optic implementation details, as well as the basic theory of how chirped-pulse phase-sensitive reflectometry can allow a better determination of the wind speed over other distributed sensing systems (2.2). The following section (3) states the details of the experiment developed, whose results are offered and discussed in section number 4. We summarize the conclusions of the article in the last section.

2. Working principles

2.1. Hot-wire anemometry

The present work relies in the basic principles of hot-wire anemometry. That is, the phenomenon of forced convective heat transport which takes place around an electrically heated, thin conductive wire. Convective flow and heat transport is a complex topic but, for many purposes, an approximate model can be applied. In this simplified model, some details such as the wire aspect ratio, fluid compressibility, non-forced convection or the variations in the thermal energy stored in the wire are omitted (this would only be relevant for the high frequency response, and may be essential when studying turbulent flows). The anemometer wire is then characterized by its electrical resistance R, which depends on the fabrication material and its dimensions, and the surface area exposed to the fluid S. In our system, the wire is replaced by a metal-coated sensing fiber. A current is fed through the metallic coating of the fiber, and the temperature evolution is read in the fiber core. The power dissipated by the conducting filament is $P = IR^2$ where I is the heating electric current. In a fully developed steady state, this dissipated power is totally delivered to

its surroundings by means of convection around its surface (whenever the thermal conductance of the fluid is negligible). This process can be described approximately by the Newton's law of cooling [2, 23]:

$$P = h(u)\, S\, (T_{\mathrm{w}} - T_{\infty})\,. \tag{1}$$

Here T_{w} is the temperature of the wire and T_{∞} is the temperature of the surrounding fluid, far enough from the heat source. The *convective coefficient*, $h(u)$, depends on the flow speed u, on the geometry of the system and on a set of thermal and dynamic coefficients characteristic of the considered fluid and flow regime, e.g. its viscosity or the Reynolds number. The exact functional form of $h(u)$ has already been modeled considering more complex, theoretical or semi-empirical fluid dynamics concerns [24]. Many detailed equations have been proposed and extensively studied within the HWA literature, such as the commonly employed King's law [1]. However, there is no universal expression for this dependence, and for actual measurements a device-specific calibration curve turns out to be mandatory, due to the sensitivity of the thermal response to the aforementioned geometric and construction parameters. Usually, an exponential or power law fits adequately to the measurements, depending on the variables employed. Note that, in general, an angular factor may be included inside $h(u)$, accounting for the relative orientation of the fluid flow and the wire [25, 26]. In our case, this factor has also been omitted, since the dissipated power and the fraction of volume occupied by the fiber are both considerably small. A more careful study should allow evaluating the angular dependence of the flow on the sensitivity. Schemes to actually measure the flow direction can also be put forward [27], however this is out of the scope of the present study. Anyway, it is clear that through Eq. (1) it is possible to calibrate the sensor response and to correlate the speed u of the fluid with either the temperature of the wire or the dissipated power, provided that the other factors remain constant.

The underlying mechanism of *constant temperature anemometry* (CTA), the most frequent approach in traditional (electronic) HWA, consists in keeping the fluid-wire temperature *drop* $(T_{\mathrm{w}} - T_{\infty})$ constant and monitoring the electrical heating power P required to do so. The technique comprises an electrical circuit that compensates the variations of the temperature of the hot wire over time. Provided that the electrical resistance depends on temperature, a variation of the wire temperature due to the forced convection naturally leads to a variation of the electrical current going along it. This automatically restores its usual temperature and resistance values. The increase or decrease of the current demanded by the wire allows to record the wind speed, after a proper calibration.

The purpose of the chirped-pulse ΦOTDR setup in our fiber-optic implementation of the HWA is to register the temperature variations inside the fiber while a constant power P is dissipated as heat to the flowing air. This power is delivered by an electrical current fed into the fiber metal coating. By periodically switching the current on and off, the induced temperature cycles can be distinguished from natural background variations. Thanks to the forced convection principles, the amplitude of these cycles is tightly coupled to the wind speed, motivating the proposed anemometer. The temperature difference between the heated and non-heated steady states of the fiber is equivalent to the term $(T_{\mathrm{w}} - T_{\infty})$ in Eq. (1), provided the cycles are slow enough (for a given wind speed and heating power) to actually allow the system reach a quasi-steady state. Since the temperature measurements are done for every single point of the whole fiber, this allows to recover the thermal response of each point, and through a proper calibration of $h(u)$, the local wind speed. Note that the off periods of the current signal are fundamental to establish a reference non-heated state for the evaluation of the true temperature drop. In addition, the heating modulation serves to easily filter out the ambient temperature variations in time as well as other possible non-correlated sources of drift in the setup (e.g. laser phase noise, etc.). In our implementation, only the components at the frequency of the switching current are analyzed, making the system robust against all these deleterious effects.

It is interesting now to look at the dynamic response of the heating and cooling cycles. We show

here that the direct integration of Eq. (1) leads to the characteristic exponential time-response of heating/cooling bodies, which may serve as a reference dynamic model. In this model, to characterize the heating wire response (in our case, the metal-coated fiber), we need to introduce its heat capacity, which is defined as $C = \mathrm{d}E_\mathrm{w}/\mathrm{d}T_\mathrm{w}$, where E_w is the thermal energy stored in the wire. For a compound wire, such as the optical fiber used in our experiments, we will consider an effective heat capacity (C_eff), which will represent the effect of all the contributions coming from the different materials in the structure. Now we can relate the power loss to the temperature of the body under study through its heat capacity ($P = -\mathrm{d}E_\mathrm{w}/\mathrm{d}t = -C\,\mathrm{d}T_\mathrm{w}/\mathrm{d}t$). Inserting this into Eq. (1), it is trivial to arrive at the following dependence of the wire surface temperature on time (t):

$$T_\mathrm{w}(t) - T_\infty = A\, e^{-kt}, \tag{2}$$

with $k(u) = h(u)S/C$. Note that negative values of the amplitude parameter $A(u)$ account for the response during heating up, while positive values account for the response during cooling. It can be easily seen that the time constant of the process ($\tau = 1/k$) will also depend on the speed of the fluid through $h(u)$. Even though this quantity may, in principle, be used for wind speed measurements, we will see later that in our implementation it provides fairly inaccurate results. However, by combining this expression with Eq. (1), we will show that the measurement of the time constant can be employed in order to estimate a value for C_eff, which should lay in the range of values of heat capacity of the different components embedded into the metallic-coated fiber. This will allow to validate the measuring principles here presented.

2.2. Fiber optic implementation of a hot-wire anemometer

The principles of HWA explained above can be adapted to implement an anemometer based on optical fiber sensing of the induced temperature changes, resulting in both point-sensors [28–33] and distributed ones [27, 34]. As in conventional HWA, the sensing optical fiber has to be artificially heated up. Accordingly, its temperature balance will be determined by convection (Eq. (1)), which is in turn related to the surrounding fluid speed. Consequently, the fiber temperature carries information about the speed of the wind drifting around it. The system presented in [34], which is based on a Brillouin optical time domain analysis (BOTDA) sensor, provides wind speed measurements in the range of 1–10 m/s with spatial resolutions in the order of 1 centimeter. The anemometer developed in [27] employs optical frequency domain reflectometry (OFDR) to probe a 70 m-long grid of fibers. It was demonstrated that the flow rate, position and direction of several air jets could be determined, with a spatial resolution of just a few microns. However, these demonstrated distributed methods are far from reaching the specifications needed by DLR: their temperature resolution is relatively low (not below 0.1 K), which makes impossible for them to provide, in short acquisition times, high sensitivity wind speed measurements along kilometers of fiber, unless the injected heating power is unrealistically high. Thus, if the dissipated power has to be lowered to more realistic values, a method with much higher temperature resolution is needed.

To monitor the temperature distribution of the optical fiber, we propose a method based on phase-sensitive optical time domain reflectometry (ΦOTDR). The core of the technique is the analysis, in the time domain, of the Rayleigh-backscattered light generated by an intense and coherent light pulse traveling along the core of a conventional optical fiber. The back-scattered light signal or trace presents a speckle-like pattern produced by the interference of the light reflected at millions of sub-wavelength size scattering centers. This trace constitutes a fingerprint of the physical state of the fiber: it remains constant if the fiber and measuring conditions do not change over time, but is locally altered under variations in the local fiber refractive index or scattering centers positions, typically related to strain or temperature variations. In this time-domain implementation, the time of flight of the pulse in the fiber naturally correlates to the fiber position through the group velocity of the light in the fiber ($z = ct/(2n_\mathrm{g})$). Therefore,

whenever an external perturbation modifies the refractive index or the distance between scattering centers at a certain spot in the fiber, the optical *echo* detected at its input end will be altered at the corresponding time delay in the trace [35, 36].

In a conventional ΦOTDR sensor, a local modification of refractive index is manifested in the shape or intensity of the traces, as the changes in phase of each reflection of the pulse affect the local interference outcome. However, the intensity response at that position varies non-linearly and even non-monotonically with the refractive index change, which makes it considerably complex to retrieve the actual value of the applied stimulus [37]. Although some methods can in principle track these variations (if they are slow enough) and provide sensitive measurements, they do not offer information about aspects as relevant as the sign of the applied perturbation [38]. Some techniques have been developed in the last years that can retrieve the sign and magnitude of the perturbation by performing intensity-only detection . For example, in their publication, Liehr et al. [39] achieve true strain/temperature measurements (preserving the perturbation sign) by alternating pulses of slightly different wavelengths. However, this technique necessarily multiplies the acquisition time, limiting the dynamic performance of the sensor. In addition, there exist in the state of the art other high performance temperature DOFS based on different sensing principles, such as Raman scattering [40, 41], Brillouin scattering [42], or even combinations of multiple techniques [43]. While these techniques may be able to provide absolute temperature measurements, they generally provide low resolution temperature measurements, and are not well adapted to dynamic monitoring. This poses serious limitations to their use in distributed anemometry.

Recent research carried out by the authors [21] has demonstrated an important advantage by imprinting the ΦOTDR probe pulses with a linear variation in its instantaneous frequency (*chirp*). With chirped pulses, a local temperature/strain increase in the fiber is translated into a local time shift of the trace fingerprint, while preserving the sign information. For pulse lengths in the order of meters, the refractive index sensitivity of this technique turns out to be in the order of 10^{-8}, which translates into mK/nε temperature/strain sensitivities. Once each trace is acquired, a comparison with the previous trace is performed through the calculation of local correlations. This procedure allows to track the local delay imprinted on the trace and, therefore, the temperature or strain evolution. More importantly, the relationship between the applied perturbation and the obtained delay is linear, with a proportionality constant related to the chirp applied to the pulse [21].

Overall, the proposed method provides a linear response (which the traditional intensity-based ΦOTDR lacks) and enables the system to perform single-shot measurements of small refractive index variations, with spatial resolutions in the order of meters over distance ranges of several tens of kilometers [44]. Such a result implies not only a fundamental advantage over intensity-based ΦOTDR, but also opens up an interesting room for improved or even new applications. For example, when working in intrusion detection via ΦOTDR, a further analysis of the measurements (beyond simple thresholding of the ΦOTDR data) is frequently performed. Typically, pattern recognition and machine learning strategies are applied [45, 46]. Such techniques generally work much better with a high-fidelity input, and keeping the sampling rate as high as possible.

For our anemometry setup, we are interested in the sensitivity of the technique to temperature variations. The expression giving the local trace delay δt due to a change in temperature δT at the point z is [21]:

$$\delta t(z) = 6.92 \times 10^{-6}\,\mathrm{K}^{-1}\,\frac{\nu_\mathrm{o}}{\delta\nu}\,\tau_\mathrm{p}\;\delta T(z), \tag{3}$$

where ν_o is the central frequency of the emitted pulse, $\delta\nu$ is the chirp frequency span (i.e, the total frequency bandwidth of the pulse), and τ_p is the employed pulse duration. As it can be seen in the above expression, this method presents a tunable sensitivity which can be easily controlled by means of the applied frequency spread of the pulse. For a typical bandwidth of several hundreds of MHz, a pulse duration of tens of nanoseconds, and a sampling rate in the order of tens of

GSPS, a sensitivity of the order of millikelvin is reached. Also, this chirp is small enough to make the effects of dispersion negligible even after tens of km of propagation, as demonstrated in [44].

Now we are interested in having a first-hand evaluation of the potential sensitivity to wind speed that can be achieved by combining the hot-wire anemometry concept with the chirped-pulse ΦOTDR. By comparing with the wind speed sensitivities already achieved along the literature, we can know the expectable wind speed sensitivity range for our setup, as it is proportional to the available temperature sensitivity. Of course, we could also take advantage of the heating power variable P, which allows to work with larger temperature changes and thus enhance the anemometer sensitivity, at the expense of a much higher power consumption of the scheme. Hence, it becomes necessary to specify the sensitivity achieved with a setup *as a function of the dissipated power*. In our case, since the dissipated power needed to monitor a certain fiber depends on the total distance to be monitored, the sensitivity should be specified as a function of the dissipated power *per meter of fiber*. This will give us a fair evaluation of the improvement given by this technique over previous techniques demonstrated in the literature. Note that, in addition to a high temperature resolution, it is also necessary to keep the acquisition time as low as possible, as otherwise the compensation of the background temperature would not be accurate enough. Rapid switching between the current-on and current-off states would provide a better estimation of the temperature drop. The chirped-pulse ΦOTDR provides both features, unlike techniques such as BOTDA, where a high sensitivity comes at the expense of a much longer acquisition time.

Some remarkable experiments such as that of Chen et al. [27] achieve systems that, with a distributed temperature sensor featuring a resolution of 0.1 K, can determine wind speeds with uncertainties down to $\approx \pm 0.08$ m/s (at a wind speed around 0.25 m/s). However, it must be noted that this impressive wind speed uncertainty comes at the expense of having temperature changes in the fiber in the order of 100 K, which implies power dissipations in the order of 5 W/m. For a typical DLR span of e.g. 40 km this would imply a total power dissipation of 200 kW, which can be considered unassumable for infrastructure operators. Enhancing the temperature sensitivity to the mK range, the power requirements to achieve a similar wind speed resolution become 100 times smaller, making the system much more attractive for transmission system operators. Of course, having a much smaller temperature change implies that the effect of the natural temperature drifts of the fiber becomes much more important. To avoid this problem, a modulation of the power dissipation is performed in our setup, allowing to discriminate the drifts from the background evolution simply by recovering the corresponding spectral components of the temperature modulation.

3. Experimental setup

The basic components of the chirped-pulse ΦOTDR experimental setup are depicted in the Fig. 1. To monitor the fiber under test (FUT), a pulse train is generated along the upper branch of the diagram. The same signal generator (SG) serves to modulate the instant frequency ($\delta\nu \approx 1$ GHz around $\lambda_o \approx 1547$ nm) of the continuous wave (≈ 50 kHz static linewidth) external cavity laser diode (LD) and to synchronously create a pulse (40 kHz) repetition rate at its output by means of a semiconductor optical amplifier (SOA), which windows a small portion of the frequency ramp modulation. An SOA is employed to shape the pulse, taking advantage of its good extinction ratio (50 dB). The selected chirp value and the digitizer speed (40 GSPS) allows to resolve temperature changes of around 2 mK for pulses of duration 100 ns. After being amplified (≈ 20 dB) with and erbium-doped fiber amplifier (EDFA) and adequately filtered (with a ≈ 0.6 nm-wide filter), the pulses are ready to probe the FUT.

The signal backscattered by the FUT through Rayleigh scattering is conditioned in the lower branch of the scheme. This makes the traces powerful enough to be successfully detected with a p-i-n high-speed photodetector (bandwidth of ≈ 1 GHz) and further digitized and processed. Fiber

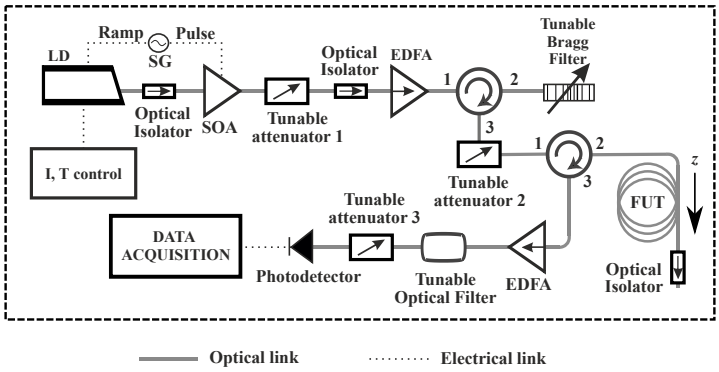

Fig. 1. Diagram of the sensor setup. The deployment of the fiber under test is shown in Fig. 2. Acronyms are explained within the text.

isolators and attenuators are inserted at several points of the setup to prevent from undesired reflections and to limit the light power, respectively. Given the length of the employed FUT and the experimental conditions, the temperature of the fiber could be acquired every 40 ms, considering 8 individual traces were averaged for each measurement in order to reduce vibration-induced noise. With this probe pulse repetition rate, monitoring a 10 km fiber requires processing around 6 GB/min in real time. This can be done with a graphic processing unit (GPU), which reduces in real time each 40 GSPS ΦOTDR trace to a 1000 points temperature trace, while the only information finally stored is the temperature distribution along time (at a rate < 4 MB/min).

In our experiment, a commercial copper-coated fiber was used (IVG Fiber Cu1300). This fiber consists of a standard single-mode core and cladding (of diameter 125 µm) coated with a (20 ± 5) µm thick copper layer. A 22 m long piece was used, while only its central ≈ 13 m segment was deployed inside a wind tunnel (see Fig. 2), suspended from 7 points (2.2 m apart from each other) with the help of 7 supporting reels. This was the monitored region, which was chosen to approximately match the nominal spatial resolution of the setup (i.e. ≈ 10 m when launching 100 ns long pulses). The extra 5 m at the ends ensure that no splices or connectors affect the tested point. A reference anemometer (RS1340) was placed at the end of the wind tunnel in order to monitor the wind speed u and to calibrate our results. Although reducing the pulse length may be unnecessary for a distributed anemometer, this technique has provided successful measurements with spatial resolutions of even 2 m [20]. However, the quality of the chirp in this regime may be compromised because of a slow operation of the SOA, which results in a parasitic chirp contribution at the pulses edges.

In the laboratory experiment, the air current was chosen to flow longitudinally with respect to the fiber due to the limitations of the employed wind tunnel and the need of installing around 10 m of fiber inside. Considering the aforementioned angular dependence of the convective efficiency, this would be the least favorable situation for sensing. Alternative deployment schemes where the fiber is fixed at every point may be advisable for wind speeds out of the range of our experiments or for particular scenarios where more vibration sources are present.

Two electrodes were connected to the fiber coating at the ends of the tested region. The total resistance of this fiber segment was $\approx 100\,\Omega$ and the electrical signal switched from 0 to ≈ 80 mA (≈ 8 V total voltage drop) at a 100 mHz rate. This implies an on-state power supply for the fiber of around 60 mW/m. According to the tolerances provided by the manufacturer of the copper-coated fiber, the heating current should produce a relatively homogeneous temperature change along the fiber distance (with variations $< 22\,\%$). If the characteristic length of the fluctuations of the metal coating thickness is smaller than the resolution cell scale, the inhomogeneities may indeed

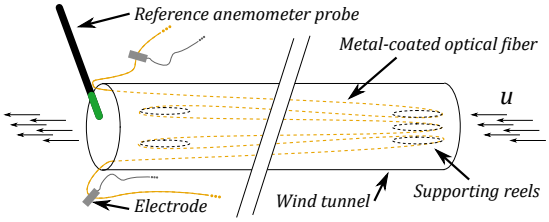

Fig. 2. Diagram of the experimental sensing fiber deployment. The coated fiber is suspended from seven points (5 cm diameter fiber reels) inside the wind tunnel.

result averaged. On the contrary, if it turns out to be larger, a calibration of the sensor after it is deployed in a real scenario would be needed to compensate these variations. On the other hand, the rotational symmetry considered above for the convection problem can also be considered realistic: for this system the *Biot number* (which represents the ratio between heat convection and conduction characteristic times) falls well under the typical homogeneity limit (0.1) [23, chapter 5]. In other words, the high copper thermal conductivity and small scale of the fiber guarantees a fast enough thermalisation of the copper coating despite the inhomogeneous convective cooling around the fiber cross section. Hence, the heat transfer from the copper layer to the glass cladding should also be radially homogeneous.

It should be noted that the tests were done with and without a lead fiber spool of 20 km with no significant variation in performance. This implies that the developed setup could easily be used to monitor a 20 km span without major deviations in the performance reported in this paper.

4. Experimental results and discussion

The feasibility of our high-efficiency distributed anemometry method is shown in the present section. The validation of the working principle is visible in Fig. 3. In this test, the temperature evolution of the fiber core in the region exposed to the wind is plotted along time. During this measurement, together with the periodic thermal excitation applied through the electric current (≈ 80 mA), different wind speeds were tested in the wind tunnel. It can be appreciated that: (I) the temperature modulation amplitude is lower for greater wind speeds, as it has been suggested by the HWA model; (II) the vibrations induced by higher wind speeds may set a limit of this sensor for a certain fiber deployment; (III) the characteristic time constant of each cycle is also related to the wind speed, as anticipated by the dynamic law of heating/cooling (Eq. (2)) derived in our model.

From the conclusions shown above and the theoretical model developed in section 2.1, we can devise two methods to recover the wind-speed information from the chirped-pulse ΦOTDR measurements: the first one consists on the measurement of the temperature modulation amplitude; the second one consists on the exponential fitting of the heating/cooling processes, to determine the time constant of the process and relate it to the wind speed. Although a single cycle is enough to characterize the time constant and the amplitude, the accuracy of the results grows with the number of cycles considered. In the analysis of our experimental results, the amplitude analysis proved much more accuracy than the exponential fitting (Eq. (2)), and is the method primarily considered here. It is believed that this is related to the fact that the curve fitting process is more vulnerable to vibrations at high wind speed.

For an accurate measurement of the temperature modulation amplitude, we propose to compute it in the frequency domain. This allows to focus on the actual excitation frequency, bypassing the slow drifts (coming from the laser source instabilities; slow, mK-scale fluctuations of the ambient temperature; etc.) and the fast variations due to noise at the trace level, mainly related to vibrations in the sensing fiber. For this purpose, a fast Fourier transform (FFT) of the measurements

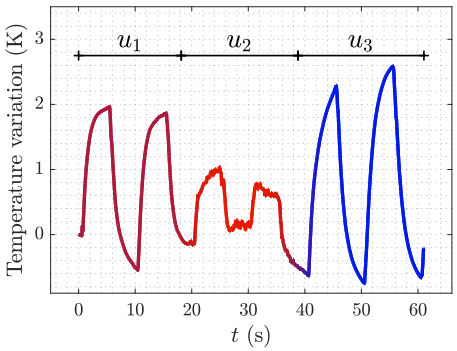

Fig. 3. Demonstration of the working principle which allows to perform fast wind speed measurements. The temperature evolution of the fiber is plotted along a few driving current cycles ($\approx 80\,\mathrm{mA}$), while the wind speed inside the tunnel was configured at three different values: $u_1 \approx 0.6\,\mathrm{m/s}$, $u_2 \approx 1.9\,\mathrm{m/s}$, and $u_3 = 0\,\mathrm{m/s}$. It is appreciable the time-response of the system is conditioned by the wind speed.

acquired for different wind speeds was performed. Each processed time series comprised 24 complete cycles taken at 100 mHz along 250 s. The FFT results are shown in the Fig. 4 (left), where the magnitude at the driving frequency corresponds to half the peak-to-peak temperature difference ($\Delta T_\mathrm{w}(u)$). The curves appear in order, from low wind speed values (bluish) to high values (reddish), as was expected from the discussion of Fig. 3. The relation between the air speed (as given by the reference anemometer) and the magnitude of the fundamental peak of the FFT spectrum is shown in Fig. 4 (right). We can see that a measurement of the FFT peak magnitude can provide a value for the air speed u through the displayed calibration curve. For our system, the best simple fit of the dependence $\Delta T_\mathrm{w}(u)$ (within the speed range considered in the experiments) was quadratic. This fit corresponds to the functional dependence on u of the inverse of the convective coefficient, $h(u)$. The fitting R-squared coefficient (0.974) and the 95 % confidence bounds for the independent term are also provided for visual guidance. The span between these bounds provides an estimation of the measurement uncertainty over the selected measurement time (4 minutes): $\approx \pm 0.15\,\mathrm{m/s}$ ($\delta u \approx 0.31\,\mathrm{m/s}$ around $u = 0.25\,\mathrm{m/s}$). However, it should be noted that the confidence bounds strongly depend on the measurement time. This span shows an approximately linear decay as the length of the time series considered for the FFT calculation is incremented. This trend implies an almost zero width of this span for integration times around 15 min ($\approx$ 80 cycles) in our configuration, letting the system reach its minimum uncertainty.

A natural definition for the sensitivity is the inverse of the slope of the calibration curve of the FFT peak magnitude vs u, represented in Fig. 4 (right). This definition has been evaluated and plotted in red in the same figure (right axis). When measuring around $u = 0.25\,\mathrm{m/s}$, the absolute value for this sensitivity is 1.8 $(\mathrm{m/s})\,\mathrm{K}^{-1}$, which is almost two orders of magnitude higher than that reported by [27]. Note that increasing the value of power dissipation (and consequently the temperature modulation) would allow to achieve higher u sensitivity. In such case, it should be taken into account that upscaling the power density factor substantially (one or two orders of magnitude higher) may cast the convective problem out of our model: the natural convection may become non-negligible in this case and some corrections may come into play. In addition, for most realistic applications such a high sensitivity would probably not be required. In other words, the estimation provided sets a comparison of this system with the state of the art, but is meaningless in realistic terms. As counterpart, we have shown that we can lower the heating power density roughly two orders of magnitude (from 5.4 W/m to 60 mW/m) while keeping sensitivity

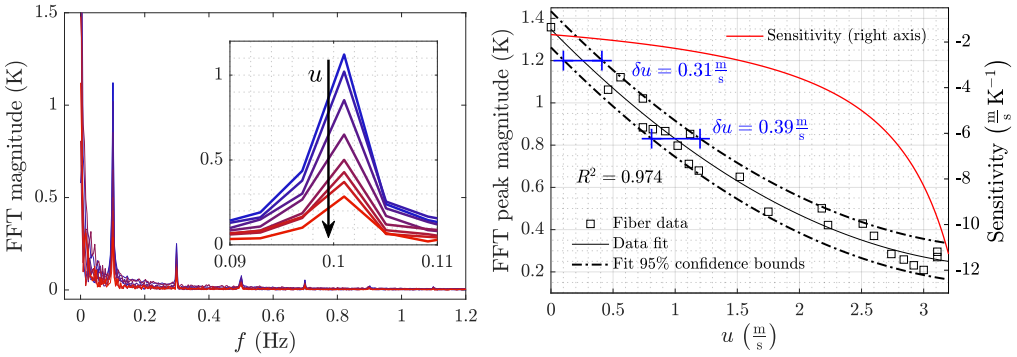

Fig. 4. Left: FFT of the cyclic exponential-like thermal time-response for several values of u. The shown FFT magnitude corresponds to half the peak-to-peak range of the time series. The value at the FFT peak corresponding to the frequency of the heating cycles (inset) and its first harmonics scale with the applied wind speed. Right: the evolution of the maximum at 100 mHz for different reference anemometer readings has been plotted and fitted.

values significantly close to those demonstrated in earlier literature. Thus, the real contribution of the present work is, more than an improvement in sensitivity, the power density reduction that it demonstrates, as it makes possible to make truly distributed flow speed measurements over distances of tens of kilometers and with affordable power dissipation.

It should also be considered that the data dispersion is mainly due to the vibrations of the fiber, as it was only suspended from 7 points while being exposed to the air flow. Thus, a more robust implementation should help keeping separated the mechanical and the thermal effects of the wind on the tested fiber, making possible to properly measure its temperature with the accuracy provided by the chirped-pulse ΦOTDR interrogator. For example, we suggest attaching the sensing fiber to a thick (more massive and rigid) cable. Such a system would naturally be immune to vibrations in the time-scale of the heating-cooling cycles, which interfere in the temperature tracking. In such a system, higher frequency vibrations would be present, but this would only affect at trace level, and its impact on wind speed measurements could be reduced by increasing the number of traces averaged per temperature distribution acquired. On the other hand, externally attaching the coated fiber to such a structure would avoid reducing the convective efficiency with isolating jackets, hence avoiding an impact in the anemometer wind speed resolution or power consumption. In addition, it is also worth mentioning that the anemometer sensitivity is related to the orientation of the fiber with respect to the wind direction. As such, the tests shown here provide the worst convection efficiency, implying that this would be the worst sensitivity attainable with this technique.

In the Fig. 5 (left) we show the cooling-down and heating-up curves corresponding to the 24 consecutive cycles of a particular time series (obtained for a wind speed of 0.56 m/s). The data has been processed to discard the slow room temperature drift and to show the repetitions of each part of the cycle aligned together. This same procedure was applied to the measurements acquired for different wind speeds. For each time series, the average cooling-down and heating-up curves were calculated and fitted to exponentials, as shown in our model (Eq. (2)).

It should be noted in advance that in our implementation the time constant of the exponential does not provide as good accuracy as the one obtained using the FFT. Thus, we do not use this technique for performing actual measurements of wind speed. Still, these measurements allow us to make a validation of the self-consistency of the measurement method and the model. This is done by considering the results from the FFT peak magnitudes and the dynamic decay time measurement together. According to the model given in section 2.1, we can estimate the fiber

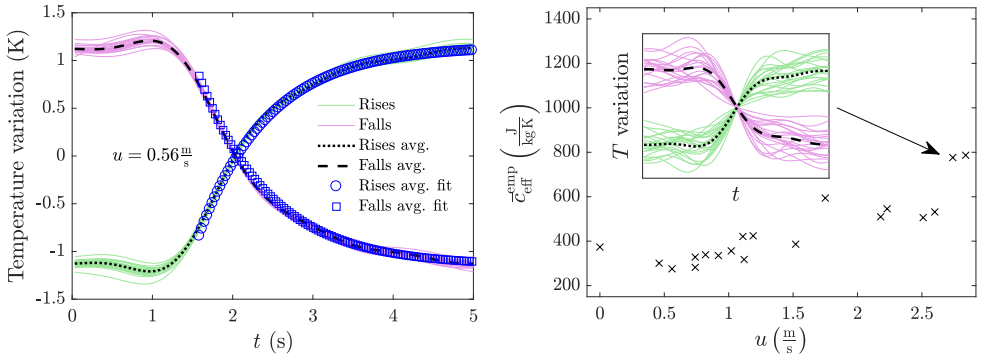

Fig. 5. Left: example of the thermal switching curves considered for the exponential fits. The data corresponds to a set of 24 consecutive cycles registered under a wind flow of speed 0.56 m/s. The corresponding fittings (blue markers) was performed on the average curves (dashed lines). Right: $\bar{c}_{\text{eff}}^{\text{emp}}$ as obtained for different wind speeds from the fitting time constant and the FFT magnitudes; the disagreement at high wind speed is due to the inrush of fiber vibrations in the temperature measurements (inset).

effective heat capacity (C_{eff}) from these two measurements. From the steady states model (Eq. (1)) we can write down the convective coefficient as $h(u) = P/(S\,\Delta T_{\text{w}}(u))$. On the other hand, from the dynamic model (Eq. (2)), we have that $h(u) = C_{\text{eff}}/(S\,\tau(u))$. Putting the expressions together and considering the *specific heat capacity* definition for a body of mass m ($\bar{c} = C/m$), we can end up obtaining an empirical result for $\bar{c}_{\text{eff}}^{\text{emp}}$ at each wind speed setting. This value should be constant for all the measured wind speeds, as it is a property of the fiber materials in the coated fiber. The resulting heat capacities are plotted in Fig. 5 (right). Although the dispersion is high, for u in the range from 0 to 1.5 m/s, the empirically-obtained heat capacity remains approximately constant, with values in the order of $\approx 400\,\text{J/(kg K)}$. We can now compare this result with a theoretical estimation using the nominal properties of the components of the fiber and their relative masses. By taking the copper and fused silica densities (ρ_{i}) and specific capacities ($\bar{c}_{\text{i}}$) from tables [23] and considering the geometry and specifications of our sensing fiber (see section 3), we reach a theoretical estimation of $\bar{c}_{\text{eff}}^{\text{theo}} = \sum \bar{c}_{\text{i}}\, m_{\text{i}}/m_{\text{total}} \approx 500\,\text{J/(kg K)}$. The empirical result obtained for all the measurements is consistently smaller than the simple theoretical estimation shown above (which is related to the high glass heat capacity), but turns out to be quite close to the heat capacity of pure copper (385 J/(kg K)), and certainly within the range of expectable values. In addition, the fact that this empirical result keeps reasonably constant and within the expected range for wind speeds up to 1.5 m/s validates the consistency of the technique and the model. For high wind speeds (> 1.5 m/s), however, as it is shown in the inset of Fig. 5 (right), the vibration induced on the fiber is so high that the exponential fitting of the acquired data becomes strongly unreliable, and so do the experimental time constants recovered in these conditions. The noise added by the mechanical vibrations makes the measurement not representative of the actual temperature evolution, disrupting the exponential decay shape and leading to wrong values of $\bar{c}_{\text{eff}}^{\text{emp}}$. Lastly, it should also be considered that the disagreement of the empirical and theoretical values (even for low wind speed values) might be partially related to the simplicity of the used model.

5. Conclusions

In this work, a first demonstration of a fiber-optic distributed anemometer based on chirped-pulse ΦOTDR technology has been presented. This technology provides dynamic distributed

temperature measurements with high sensitivity (mK resolution), which provides the means to precisely track the convective heating/cooling of a metal-coated fiber exposed to an air flow while being periodically heated through Joule effect. The measurement of the heating cycles allows to extract wind speed information through simple calibration processes. Some of the parameters can be tuned in order to adaptively optimize the anemometer response: for example, higher resolution values in the wind speed determination can be achieved at the expense of more electrical power dissipation along the fiber. In terms of spatial resolution and range, our proof of principle demonstration has shown a spatial resolution of 10 meters over a distance range of roughly 20 km. However, considering recent studies on the viability of combining the chirped-pulse ΦOTDR system with distributed Raman amplification, the present work could easily be the basis for a distributed anemometer capable to operate in ranges reaching up to 75 km [44] with similar resolution values (10 m) as the present work, provided the availability of computational means which fit the data-rate estimations stated in section (3). Alternatively, other lower bandwidth implementations of distributed hot-wire anemometer based on similar temperature measurement principles (such as the one proposed in [39]) could be developed.

It has been shown that the high temperature sensitivity of our measuring system allows to achieve comparable wind speed uncertainty to former systems demonstrated in the literature using the same HWA principle [27] but in our case requiring two orders of magnitude smaller dissipated power. In addition, the fact that our system is modulated leads to a more robust behaviour against the fiber temperature drifts. Our system presents therefore a huge leap in applicability for several potential applications, particularly considering dynamic line rating (DLR).

Funding

This work was supported by: the ERC through project U-FINE (gr. 307441) and a FP7 ITN ICONE program (gr. 608099); the EC H2020 and Spanish MINECO (project DOMINO, ERA-NET Cofund Water Works 2014 call); the FINESSE project MSCA-ITN-ETN-722509; the MINECO (projects TEC2013-45265-R, TEC2015-71127-C2-2-R, a FPI contract and a “Ramón y Cajal” contract); the regional program SINFOTON-CM: S2013/MIT-2790; and the University of Alcalá (FPI contract).